Use of radar rainfall estimates and forecasts to prevent flash flood in real time by using a road inundation warning system

Pierre Antoine Versini

Use of radar rainfall estimates and forecasts to prevent flash flood in real time by using a road inundation warning system

Versini, P.-A.
CRAHI-UPC, Barcelona, Spain

Abstract

Important damages occur in small headwater catchments when they are hit by severe storms with complex spatio-temporal structure, sometimes resulting in flash floods. As these catchments are mostly not covered by sensor networks, it is difficult to forecast these floods. This is particularly true for road submersions, representing major concerns for flood event managers. The use of Quantitative Precipitation Estimates and Forecasts (QPE/QPF) especially based on radar measurements could particularly be adequate to evaluate rainfall-induced risks. Although their characteristic time and space scales would make them suitable for flash flood modelling, the impact of their uncertainties remain uncertain and have to be evaluated.

The Gard region (France) has been chosen as case study. This area is frequently affected by severe flash floods, and an application devoted to the road network has also been recently developed for the North part of this region. This warning system combines distributed hydro-meteorological modelling and susceptibility analysis to provide warnings of road inundations. The warning system has been tested on the specific storm of the 29-30 September 2007. During this event, around 200 mm dropped on the South part of the Gard and many roads were submerged. Radar-based QPE and QPF have been used to forecast the exact location of road submersions and the results have been compared to the effective road submersions actually occurred during the event as listed by the emergency services.

Used on an area it has not been calibrated, the results confirm that the road submersion warning system represents a promising tool for anticipating and quantifying the consequences of storm events at ground. It rates the submersion risk with an acceptable level of accuracy and demonstrates also the quality of high spatial and temporal resolution radar rainfall data in real time, and the possibility to use them despite their uncertainties. However because of the quality of rainfall forecasts falls drastically with time, it is not often sufficient to provide valuable information for lead times exceeding one hour.

1- Introduction

Mediterranean regions are subject to violent flash floods, resulting in heavy economic damages, estimated at a billion Euros in France over the last two decades Gaume et al., 2004 and, in some cases, human casualties, as illustrated by the recent events in Nîmes (1988), Vaison-la-Romaine (1992), Tarragona (1994), Biescas (1996), Corbière (1999), Alger (2001), Gard (2002) and Var (2010). Flash floods are identified as the consequence of an intense rain event producing several hundreds of mm in few hours (Creutin and Borga, 2003; Collier, 2007; Younis et al., 2008). During this type of event, spatial and temporal variability of rainfall appears to be the main factor controlling the hydrological response (Chancibault et al., 2007; Le Lay and Saulnier, 2007) and this evolution is very difficult to predict. Flash floods typically occur in quick response watersheds for two main reasons: (i) a short concentration time due to the size generally under few hundreds km^2, (ii) flood flows that are essentially composed of surface runoff water or at least fast responding runoff processes (Creutin, 2009). That makes very difficult for emergency management services to anticipate and deliver flash flood warnings in real time.

This is particularly true concerning the road network that could be strongly affected during flash floods. In a situation of risk, the state of the road network has appeared as a major concern within these affected regions for two main reasons. First, many flash flood victims are in fact motor vehicle passengers trapped in inundated roads (Staes et al., 1994; Bourque et al., 2007). Second, emergency services require a clear overview of possible road conditions in order to efficiently plan interventions and identify safe access or evacuation routes.

Based on these considerations, a Road Inundation Warning System (RIWS) for flash flood prone areas has been recently developed and tested on the North part of the Gard Region (France) frequently affected by flash floods (Versini et al., 2010a). Coupling a susceptibility analysis of river road intersections (representing one part of the vulnerability to flooding) based on geographical information (Versini et al., 2010b and a) distributed hydrological model, the RIWS has provided promising results. Tested on real cases, it was able to correctly assess the inundation risk with an acceptable level of accuracy. Nevertheless, this previous work has opened many ways of investigation before being applied in a decision support system. First, operational services interested

by the RIWS has advised to study its possible application on a territory where it has not been calibrated to test the transferability of the whole prototype. Secondly, as the spatio-temporal distribution of rainfall has appeared to have a major influence on the state of the road network, the hydrological model had to be adapted to take into account distributed rainfall products, especially those based on weather radar. Indeed, one important feature of road submersion is the significant number of targets (that could be located on very small watersheds) regarding the limited coverage of rain and stream gauges, making this framework close to ungauged conditions. For example, the Gard region (580 km^2) is covered by 38 stream gauges for 2480 crossing structures.

Accurate quantitative precipitation estimates (QPE) are also crucial for operational flash flood forecasting. Ground-based operational weather radars currently appear as the only instrument able to provide valuable information with a high spatial (1 km^2) and temporal (tens of minutes) resolution. The density of automated rain gauges network is generally too low and not adapted to flash flood short time and space resolutions. In this case rainfall estimation uncertainties are still a major factor limiting the accuracy of rainfall-runoff modelling (Moulin et al., 2009). Moreover, rainfall estimated using satellite remote sensing is still under development and not sufficiently advanced to be used in an operational mode. Consequently, radar QPE is accepted as one of the most reliable data that can be used for hydrological applications (Corral et al., 2000; Borga, 2006; Cole and Moore, 2008).

This is also the case concerning quantitative precipitation forecasts (QPF). Although few works have focused on using QPF based on weather radar data, results show significant improvements in the quality of forecasted hydrographs (Corral et al., 2000; Dolciné et al., 2001; Berenguer et al., 2005; Borga, 2006; Boudevillain et al., 2006; Van Horne et al., 2006; Vivoni et al., 2006; Cole and Moore, 2008). These radar-based QPF are usually limited to forecasting time ranging from 10 to 120 minutes. Tested on rather large basins (from hundreds to thousands km^2), the anticipation of flow peak could be estimated, with enough quality, with a lead-time for up to few hours. It represents a notable improvement for fast response basins such those in Mediterranean regions. It is also recognized that the nature of the event has an important effect on the quality of the forecasted flow estimates. In Collier, 2007) a review is made to study how flash floods are forecasted considering the limitations and uncertainties involved in both meteorological and hydrological models of the forecasting system. The author

concludes the possibility to deliver valuable information from a flash flood risk management point of view limited to a lead-time of two hours.

This paper deals with a practical application of this statement. The main objective of the present work is to test the use of radar-based QPE and QPF on a specific hydrological application devoted to the road network. The spatio-temporal variability information provided by the radar based precipitation estimates and forecasts will be tested using the RIWS. The warning system will be firstly transported and adapted to a new basin located in the South part of the Gard region. It will be then applied to reproduce the specific storm of 29-30 September 2007 during which 19 roads were submerged. Predicted road inundations will be compared to what actually occurred. This will allow us to assess both the transfer of the RIWS on an area where it has not been calibrated, and the use of the available QFE and QPF products for flood forecasting in a framework reproducing operational conditions.

This paper is organised as follows: the next section presents the scope of study in more detail, including a description of the area of study, the rainfall products, and the RIWS. Section 3 describes the methodology applied to: i) transfer and test the RIWS to the new domain, and ii) test the information provided by the QPE/QPF, and their benefits in the detection and prediction of inundated roads. The results obtained during the 29-30 September 2007 storm are presented in Section 4. Finally, Section 5 will conclude on both topics presented in Section 3.

2- Presentation of the case study

2-1 The Gard region

The Gard region (South of France) was used to develop and test the RIWS because it is frequently affected by severe flash floods (Delrieu et al., 2005; Gaume et al., 2009). This region has a typical Mediterranean climate characterized by frequent and very heavy storm events occurring especially in autumn. The 1 in 10 year daily precipitation exceeds 100 mm on the plateaus (eastern part) and 150 mm in the mountainous western part of the area (CNRS/INPG, 1997). Single storm events can produce locally hundreds of millimetres within few hours.

During these storms, roads are often flooded. Significant inundation occurs at least once a year on average on the same vulnerable section of the road network. 40% of the

151 victims of floods in the Gard during the last 50 years were motorists Antoine et al.,
152 2001. During the extreme September 2002 flood (Delrieu et al., 2005; Ruin et al.,
153 2008), about 200 emergency vehicles were seriously damaged or destroyed by the
154 flows. For these reasons, the monitoring of the road network during flash flood events
155 has become a major concern for management services. The inundated road sections are
156 now systematically inventoried during or after every major event by the local services in
157 charge of road maintenance. It is based on these considerations that the first attempt
158 represented by the RIWS has been conducted to forecast the possible inundated road
159 (Versini et al., 2010a). A summary of this prototype will be described further (Section
160 2.3).

161 This study mainly focuses on the southern part of the Gard region (Fig. 1) where both
162 Vidourle and Vistre watersheds join the scrubland of La Camargue (swamp zone of the
163 Rhône Delta) before entering into the Mediterranean Sea. Both watersheds are located
164 outside the calibration area of the RIWS and differ from this one from a geographical
165 point of view. The Vidourle basin has a drainage area of 833 km^2 and an altitude
166 ranking from 3m to 770 m. This watershed is essentiality covered by rural landscapes:
167 vines and forest. The Vistre watershed (476 km^2) is quite different with lower altitudes
168 (4 m to 200 m with an average altitude of 70 m) and a more urbanized land with the
169 presence of the city of Nîmes (150.000 inhabitants) upstream of the basin. Because of
170 this very flat topography, river floodplains are wider and easily inundated.

171

172 2-2 Meteorological and Hydrological data:

173 Known as an area very sensitive to flash flood, the Gard region is covered by a dense
174 network of rain gauges and two weather radars (Nîmes and Bollène). Rain gauge and
175 discharge data used in this study were collected and analysed in the framework of the
176 Cevennes-Vivarais hydro-meteorological observatory (OHM-CV,
177 www.lthe.hmg.inpg.fr/OHM-CV). This observatory is a research initiative aiming at
178 monitoring and understanding intense Mediterranean storms and flash floods (Delrieu,
179 2004). On the other hand, two different services are in charge of hydro-meteorological
180 warning and are authorized to deliver QPE and QPF for flood management in real-time:
181 (i) the service of flood prevention (SPC for “Service de Prévention des crues” in
182 French) is the local service in charge of flooding prevention specially devoted to the

183 Gard region, and (ii) the national meteorological agency, Meteo France (MF hereafter),
184 that delivers radar-based rainfall maps for the whole country. Processing of this
185 different data is briefly described below.

186 *2.2.1 Cevennes-Vivarais hydro-meteorological observatory data*

187 Seventeen automatic hourly rain gauges are located within or close to the Vidourle and
188 Vistre watersheds. They have been set up for flood forecasting purposes. While the
189 density of about two gauges per 100 km^2 is quite good, it could not enable accurate
190 estimations of rainfall intensities by spatial interpolation at time and space scales suited
191 to flash flood dynamics: sub-hourly time step and kilometric scale (Moulin et al., 2009).
192 OHM-CV uses an ordinary kriging technique (Journel and Huijbregts, 1978), using a
193 spherical variogram model, to interpolate the rain gauge measurements and map rainfall
194 rates at a 15-minutes time step and 1 km^2 grid covering the area of study Lebel et al.,
195 1987. As rain gauge data are only available at hourly time step, constant rainfall
196 intensities were assumed for the entire hours.

197 The Vidourle catchment is well instrumented with numerous hourly stream gauges.
198 Three dams (Ceyrac, Conqueyrac, and La Rouvière) are located in the upstream part
199 and four gauge stations (Quissac, Vic-Le-Fesq, Sommières, Marsillargues) on the
200 principal stream in the Vidourle valley (see Figure 1). On the other hand, the Vistre
201 catchment is poorly instrumented with only one station located at the watershed outlet
202 (Le Cailar).

203

204 *2.2.2 Gard region data*

205 Complex SPC inundation forecasting system Bressand, 2002 is able to deliver valuable
206 spatial rainfall intensity at the 1km^2 scale every 5 minutes. Although this system has
207 been created by the private company REAH®, some basic elements can be explained on
208 the processes involved to correct and generate radar images Ayral, 2005. The Gard
209 region is divided into 5 windows corresponding approximately to the five main basins
210 of the region (Vistre, Vidourle, upstream Hérault, Gardon and upstream Cèze, Gardon
211 and downstream Cèze). In each window, the radar maps are specifically adjusted with
212 the rain gauge measurements using a calibration factor (FC). This coefficient is
213 calculated every 5 minutes using the three last measurements (Eq. 1). It usually varies
214 between 0.5 and 3.

$$FC = \frac{\sum_{i=1}^{n} P_i}{\sum_{i=1}^{n} R_i} \quad (1)$$

Where P_i is the rain gauge measurement, R_i is the radar measurement at the rain gauge location, n is the total number of rain gauges used to adjust radar data.

Precipitation forecasts are also calculated for different lead times varying between 5 minutes to one hour. In this case, FC used to adjust radar-based rainfall is fixed. This represents one of the weaknesses of the system. Consider the radar/rain gauge relation is constant during the storm can lead to misestimate –often underestimate- rainfall forecast.

2.2.3 Meteo France data

Meteo France produces QPE and QPF every 5 minutes over the whole country at the 1 km^2 scale based on an aggregation of radar data. After a processing chain that corrects ground clutter, partial beam blocking, VPR effects, and advection, the radar image is corrected using the rain gauges data (Tabary, 2007; Tabary et al., 2007). The principle to fit radar data to rain gauge values is also based on the use of a calibration factor. Two differences with the FC calculated for SPC data can be noted. First, this one takes into account previous rain gauge and radar measurements over a longer period. In order to give more importance to the newest values, they are multiplied by weights increasing with time. Second, a "memory" coefficient is added to constrain FC to converge to a monthly calibration factor FC_{month} when there is little rain between two events.

$$FC = \frac{\sum_{i=H-M}^{H} \omega_i \cdot P_i + C_{rec}}{\sum_{i=H-M}^{H} \omega_i \cdot R_i + \frac{C_{rec}}{FC_{month}}} \quad (2)$$

Where M is the period on which the factor is calculated, H is the lead time, P_i is the rain gauge measurement at time H, R_i is the radar measurement at the rain gauge location at time H, ω_i is the weight to filter oldest values at time H, C_{rec} is the memory coefficient, FC_{month} is the monthly coefficient.

QPF are produced for different lead times ranging from 5 to 70 minutes. The method used (Juvanon du Vachat et al., 1995a; Juvanon du Vachat et al., 1995b) derives the motion field between consecutive radar scans from the distance of the mass centers of two corresponding radar echoes. The centers are assumed to be representative for individual convective cells. This motion field is then extrapolated and applied to produce future rainfall field.

2-3 The Road Inundation Warning System

The RIWS for flash flood prone area has been developed within the FLOODsite[1] project funded by the European Sixth Framework Program. It focuses on intersections between road and river networks that can be flooded during a flash flood event, and it has been calibrated and tested on the North part of the Gard region (called "calibration area" in the rest of the paper). Both components of the RIWS (susceptibility analysis and hydrological model) are briefly presented below. For a detailed presentation, please refer to Versini et al., 2010a; Versini et al., 2010b).

2.3.1 Susceptibility rating method

An inventory of past road inundations was carried out by the public agency in charge of the road management on the North part of the Gard region, outside the studied area (Lignon, 2004). As comprehensive as possible, its objective was to collect the location of the most frequent road submersions. Based on the employees' experience and memory, it contains the exact location of 167 road sections flooded (and noted) during the last 40 years on the main road network. From this inventory, four categories of susceptibility to flooding (high, medium, low, and safe) were defined. Geographical characteristics (local altitude and slope, upstream watershed area) of crossing structure have been highlighted to explain this susceptibility to flooding and allocate every road intersection in a category. Using historical road inundations and their estimated frequency of flooding, a statistical distribution of return period of flooding was calculated for each susceptibility category.

2.3.2 Hydrological model

The CINECAR hydrological model (Gaume et al., 2004) has been selected to simulate distributed discharges. Developed specifically to model flash floods, it represents the

[1] http://www.floodsite.net/

entire watershed as a network of river reaches having a simple rectangular cross-section, connected to two rectangular slopes (characterized by areas of few km^2). The US Soil Conservation Service (SCS) Curve Number (CN) model is used to calculate the evolution of the runoff coefficient on each slope during the storm event, and the kinematic wave model is used to route the flows on the slopes and through the network of river reaches. The CINECAR model has been calibrated and validated based on the discharge time series available on 12 watersheds over the period 2000-2005. Because of the lack of available radar data, OHM-CV kriged data was used for these procedures. The performance of the model was evaluated on several rainfall events with a total rainfall exceeding 100mm available on this period. Acceptable results were obtained (average Nash criterion value of 0.3) that looked comparable to those obtained in similar studies (Borga, 2008). Based on this study, it has been considered the CINECAR model depends on only two parameters: widths of the rectangular sections representing the rivers that can be fixed *a priori* and adjusted during the storm depending on the flood magnitude, and the CN that can be also determined *a priori* from an expert judgment.

2.3.3 Risk levels

Finally, every road intersection is characterized by a susceptibility category and is connected to a river reach where the discharge is simulated. These discharges are compared at each time step with the theoretical return period thresholds for two, ten, and fifty years: Q_2, Q_{10} and Q_{50}. These theoretical return periods are approximated using a regional discharge quantile estimation method, the Crupedix method Cemagref, 1980, adjusted for France. Inundation risk levels are defined based on the susceptibility category and the discharge magnitude, or only on the discharge magnitude if susceptibility analysis is not used (see Table 1). Three levels of risk are assigned: high submersion risk (HSR), significant risk (SR), and moderate risk (MR). A warning is issued when one of the thresholds is exceeded.

3- Application of the RIWS and protocol assessment

3-1 The case of the 29-30 September 2007

The rainfall event happened during the night between the 29 and 30 September 2007 and was one of the most important that occurred in the Vistre and Vidourle watersheds

over the last years. A stationary storm with a "V" shape moved from the west to the east and intensive precipitations fell on the central part of the watersheds between 22:00 and 00:00. Between 80 and 120 mm were measured on both watersheds and locally more than 200 mm. At 2:30 the Vidourle river overflowed in Sommières. Rainfall forecasts preventing this event and issued by the French meteorological agency Meteo France were quite accurate. At the beginning of the storm (20:00), they issued a moderate warning reporting "heavy rainfall storm" during the night. An average rainfall of 50 mm was forecasted on the region around Nîmes and locally more than 150 mm. Road management and rescue services were advised of possible troubles during the night.

Finally, important damages occurred during this event. Some houses and garages were submerged, and the road network was particularly affected. Nineteen roads were closed during the night by the regional services and reopened one after the other the next day. It made rescue operations difficult and has represented a major threat to lives. The fire brigade and the regional service of rescue recognized about fifty interventions due to the inundations. Despite the advice he has been given, a motorist crossed the Vidourle and was swept away by the important flow.

3-2 Methodology

The objective is to assess the use of the quantitative precipitation estimates and forecasts by the RIWS. First, a direct analysis of the QPE/QPF will be conducted to evaluate the quality of the RIWS input. Then, the RIWS has to be transferred and applied on the South part of the Gard region where it has not been calibrated. That means both susceptibility analysis and hydrological model will be assessed on a new landscape with another road network configuration. Their results will be compared to those obtained on the calibration area. Finally, RIWS will be applied on the 29-30 September 2007 storm and its results will be analysed comparing the warnings it delivers to the actually inundated roads. The three steps, direct QPE/QPF analysis, the RIWS transfer and the RIWS assessments with QPE and QPF are described thereafter.

3.2.1 Direct analysis of precipitation

Both QPE and QPF produced by both services (MF and SPC) will be compared and evaluated. Particular attention will be given to the spatio-temporal variability of the rainfall distribution. Both hyetograms and rainfall accumulation maps will be analysed

338 at the watershed scale for the Vistre and the Vidourle basins. These data will be
339 compared to kriging interpolation-based, used as reference. It is assumed that kriged
340 data correctly represent the temporal variability of the precipitation at such large spatial
341 and temporal scale. The local heterogeneities of rainfall that are not captured by the rain
342 gauge network should have a relative low impact on the mean estimated rainfall.
343 Moreover, kriged data were processed after the storms and do not include any errors
344 associated with real time data (as QPE and QPF can do). In order to study the different
345 QPE at a smaller scale more representative of small ungauged watersheds, comparison
346 between radar-based kriged data and QPE accumulations will be also drawn at the cell
347 scale ($1km^2$).

348

349 *3.2.2 Road Inundation Warning System transfer*

350 First, the susceptibility rating method is applied. Based on geographical information
351 (local slope and altitude, watershed area), the river road intersections of the Vistre and
352 Vidourle watersheds will be spread in the four categories of susceptibility (high,
353 medium, low and safe). The verification will consist in analysing the susceptibility
354 category of the road sections effectively submerged during the 29-30 September 2007
355 storm. Locally, where intersections are subjected to the same rainfall hazard, the most
356 susceptible intersections should be flooded in priority. As the susceptibility rating
357 method has been calibrated on a region quiet different from the studied watersheds, its
358 extrapolation could be inappropriate without any adjustments.

359 The transfer of the hydrological model has also to be assessed. Once the watersheds
360 have been desegregated as a network of river reaches connected to sub-basins, the
361 parameters have to be evaluated *a priori*. The widths of the river reaches have been
362 fixed to those representing a moderate discharge at the beginning of the event, and can
363 be modified during the storm according to the discharge magnitude. The key parameter
364 is the CN because it represents the evolution of the runoff coefficient value during the
365 storm taking into account the initial condition. Based on the work realized in Versini et
366 al., 2010a), an *a priori* range of CN will be used. The simulated discharges will be
367 compared to the observations available for the stream gauges of the Vistre and Vidourle
368 watersheds. In order to test the viability of this calibration *a priori*, simulated discharges
369 at the gauge stations will be also calculated using a value especially calibrated for this

event (CNcal). The simulation achieved with CNcal will represent the best performance we can expect from the hydrological model at the gauged basin scale. Every simulation will be evaluated using the Nash efficiency (Nash, 1969):

$$\mathrm{Nash} = 1 - \frac{\sum_{i=1}^{n}\left(\mathrm{Qobs}_i - \mathrm{Qsim}_i\right)^2}{\sum_{i=1}^{n}\left(\mathrm{Qobs}_i - \overline{\mathrm{Qobs}}\right)^2} \quad (3)$$

Where $Qsim_i$ represent the simulated discharges, $Qobs_i$ the observed discharges, $\overline{Qobs}$ the average observed discharge during the storm, and n the number of time steps.

3.2.3 RIWS assessment using radar-based QPE and QPF

The skill of the RIWS is assessed using a classical contingency statistical analysis. An efficient RIWS should be able to identify a large proportion of the actually observed inundations and limit the number of "false alarms" - predicted inundations that are not observed. Four criteria are therefore used to assess the performance of the proposed RIWS using the available information on the actually observed inundations:

- Probability of Detection (POD) calculated as the ratio between the number of inundated sections where a warning has been issued (Correct Warnings) and the total number of inundated road sections:

$$\mathrm{POD} = \frac{\#\,\text{Correct Warnings}}{\#\,\text{Inundated roads}} \quad (4)$$

- False alarm ratio (FAR) calculated as the ratio between the number of non-inundated sections where a warning has been issued (false warnings) and the total number of warnings delivered by the RIWS:

$$\mathrm{FAR} = \frac{\#\,\text{False alarms}}{\#\,\text{Warnings}} \quad (5)$$

- Correct negative (COR) represents the ratio between the number of non-inundated sections where a no warning has been issued (Safe) and the total number of misses:

$$\mathrm{COR} = \frac{\#\,\mathrm{Safe}}{\#\,\mathrm{Safe} + \#\,\mathrm{Misses}} \quad (6)$$

These very intuitive skill scores are computed using rainfall estimates for both services in a framework reproducing operational conditions. Four lead times (15, 30, 45, and 60 minutes) are used to test the accuracy of this data and its possible degradation over time.

In addition, the false positive rate (FPR), which is the ratio between false alarms and the number of effective non-inundated road sections (Non inundated roads), is computed. Coupled with the maximum value of POD over the event, it is used to plot ROC (Receiver Operating Characteristic) curves and evaluate the sensibility of the two-class prediction problem (flooded – not flooded). It will be particularly useful to compare the results with those obtained on the calibration area, using or not the susceptibility analysis:

$$\mathrm{FPR} = \frac{\#\,\mathrm{False\ alarms}}{\#\,\mathrm{Non\ inundated\ roads}} \quad (7)$$

4- Results

4-1 Radar-based QPE and QPF direct analysis

Rainfall accumulations during the entire storm have been computed in a window including both Vistre and Vidourle watersheds for every type of data (OHM-CV kriging, QPE and QPF from MF and SPC). They are presented in Figure 2. Scatter plots comparing radar-based QPE with kriged data are illustrated on Figure 3. Hyetograms representing mean areal intensity (with 15 minutes time step) at the watershed scale for both Vidourle and Vistre watersheds are also presented for every rainfall data in Figure 4.

4.1.1 Quantitative Precipitation Estimates

First, the spatial distribution of rainfall is studied. Despite the location of the storm core is the same for the three estimations, a marked difference in rainfall amount can be noted. The maximum accumulation exceeds 250 mm for the SPC estimates whereas it only exceeds 150 mm for MF data, respectively 200 mm for the kriging. This is also corroborated by Vic-Le-Fesq rain gauge data located where the most intense

precipitation occurred. A total amount of 175 mm was locally measured whereas 215 mm were estimated by SPC QPE, respectively 130 mm for MF QPE. It is also confirmed by scatter plots on Figure 3. At the 1km^2 scale, MF QPE have a tendency to underestimate the most intense precipitation. On the other hand, SPC QPE overestimate some of the highest accumulations measured on the Vidourle watershed, but the highest differences with kriging are located on the cells where the precipitation in interpolated. The numerous underestimations for the lowest values correspond to the Vistre watershed. As it has been shown above, SPC data is calibrated for two different geographical windows on the Vidourle and Vistre watersheds. This is strongly visible on the accumulation map with local intensities higher than 250 mm measured on the Vidourle window neighbouring a value three times lesser on the Vistre window. A short band is shared by both windows where both estimated rainfall can be compared. A significant difference around 35% is noted. It can be assumed that the FCs used during the storm tend to overestimate rainfall on the Vidourle window and/or to underestimate on the Vistre one.

Second, temporal distribution of rainfall is analysed on both watersheds. Looking at the hyetograms (Fig. 4), precipitation estimates appear to be very different from a data to another on the Vidourle basin. For example, at 22:00 the kriging interpolation-based displays a maximum intensity of 15 mm/h. It is well reproduced by the SPC estimates (17 mm/h), but widely underestimated by MF ones (10 mm/h). On the other hand, the Vistre case shows a coherent rain amount between both services and the kriged data. The maximum intensity of 38 mm/h arises between 23:00 and 00:00 on the three observed hyetograms. The large overestimation highlighted on SPC rainfall accumulation map is only slightly reflected on both hyetograms because the highest precipitations fell outside the studied watersheds.

4.1.2 Quantitative Precipitation Forecasts

QPF provided by MF and SPC are very heterogeneous depending on the studied watershed, but they all have a strong tendency to underestimate the storm intensity for the largest lead times. On the Vistre watershed, where rainfall was the highest, SPC forecasts can lose up to 30% of the maximum intensity while MF more than 60% (see Fig. 4). This time, SPC QPF show a coherent merging between both zones because the

same FC equal to 1 is used (Fig. 2). Nevertheless, despite the storm stationarity is well represented, they have a tendency to underestimate precipitation with time, especially for the highest intensities. It should be interesting to obtain additional information on the SPC QPF production to interpret them more thoroughly.

MF QPF appear to be more uncertain. Accumulation maps (Fig. 2) show a tendency to transfer the convective system to the east part of the Vistre watershed. This situation corresponds to the typical case of a regenerative system over several hours, whom the system velocity is different from the cells velocities composing the system. During a certain time, the system velocity is almost equal to zero and the storm is nearly stationary while the cells -with a lifetime shorter- are moving eastward. The method used to extrapolate motion field in operational mode capture the movement of small scale structures, typically the scale of the convective cells. In most cases this diagnosis is appropriate. Here, the displacement obtained suggests a movement towards the east, which evacuates the system too quickly and does not restore the stationarity of the regenerative system. As the forecasted system is moved to the east, it always crosses the Vistre watershed and few affect the predictions on this basin. A slight overestimation is noted for the 30 minutes forecast. Conversely, the forecasts on the Vidourle watershed are highly affected by this error. The precipitation peak that occurred at 22:00 is strongly underestimated and almost absent in the one hour forecast.

4-2 Road Inundation Warning System transfer

4-2-1 Susceptibility analysis

The road susceptibility rating method has been applied on both Vidourle and Vistre watersheds. 468 river road intersections were identified using existing river and road network GIS layers. These road intersections have been classified into the 4 categories defined above. The high susceptible category contains 12% of the river crossings; respectively 20%, 50% and 18% for the medium, low and safe categories. Susceptibility repartition of Vistre and Vidourle intersections is very similar to those obtained on the North part of the Gard where the method was calibrated (see Table 2). Although the density of linear road is quite the same (1511km/km^2 in the calibration area vs 1433km/km^2 on the study area), the density of river intersections is different: 0.87 intersections/km^2 vs 0.44 intersections/km^2. The river network is less dense on the South part of the region and the number of intersections with the road network is also lower.

490 This is due to the geographical characteristics of the region: flatter and more urbanised
491 and domesticated.

492 Concerning the twenty-three river road intersections responsible for the 19 flooded
493 roads during the 29-30 September 2007 storm, five of them are located upstream very
494 small watersheds (<1 km^2), and seven are located upstream small watersheds (<10 km^2).
495 For these watersheds, the concentration time is very short, lesser than 15 minutes for the
496 smallest ones, making difficult interventions between rainfall and its possible
497 consequences. Among the 468 river crossings identified in the study area, the twenty-
498 three inundated crossing structures are characterized by rather high levels of
499 susceptibility (see Table 2). Eight of them (35%) are included in the high susceptibility
500 category and seven (30%) in the medium one. Seven (30%) are in the low category and
501 one (5%) in the safe category. As they are characterized by a distribution of level of
502 susceptibility focused on the highest values, submerged crossing structures seem to be
503 related with the susceptibility categories defined in the calibration area (yet
504 geographically and topographically different). Considering this only event and the small
505 size of classes, it is not possible to be more conclusive.

506 *4-2-2 Hydrological model*

507 Out of the eight stream gauges located on both Vistre and Vidourle watersheds, only
508 four have registered a peak of discharge during the studied storm. All gauges of the
509 upstream part of the Vidourle catchment did not receive sufficient water to measure
510 such an increase. This is particularly true for the three dams for which the output
511 discharge remained constant during the entire storm. Finally, discharge peaks were
512 registered only at Vic-Le-Fesq (505km^2), Sommières (620 km^2), Marsillargues (798
513 km^2) and Le Cailar (440 km^2); respectively 25.8 m^3/s (0.051 $m^3/s/km^2$), 232.5 m^3/s
514 (0.375 $m^3/s/km^2$), 235.0 m^3/s (0.294 $m^3/s/km^2$), and 58 m^3/s (0.132 $m^3/s/km^2$). As the
515 discharge peak measured at Vic-Le-Fesq is very low –a specific discharge bellow 0.1 is
516 hardly represented by the hydrological model- only the three remaining gauges have
517 been kept to assess the model simulations.

518 First, these observations have been compared to the discharges obtained by the CNs
519 selected *a priori* and used in an operational mode. In the calibration process, Versini et
520 al., 2010a) have proposed a range of two CN values related to the date and the
521 antecedent rainfall amount. The beginning of the autumn season combining with a total

522 amount of antecedent precipitation lesser than 100 mm carries to use both 40 and 50 CN
523 values. Second, a calibrated CN (CNcal) has been estimated in a dichotomous way,
524 calibrating a first CN for all the sub-basins located upstream Sommières, a second CN
525 for the sub-basins between Sommières and Marsillargues, and a third one for the Vistre
526 sub-basins. The objective of this calibration is to assess the hydrological model's ability
527 to reproduce correctly the studied storm and to have an idea on the spatial distribution
528 of the CN. These simulations have been carried out using OHM-CV kriged data, and
529 both SPC and MF estimates. The different hydrographs and the Nash efficiencies
530 evaluating the simulation performance are presented in Figure 5 and Table 3.

531 The simulations obtained with the CNs selected *a priori* appear to be acceptable and
532 similar to those obtained on the calibration area (see Versini et al., 2010a). They are
533 particularly reliable on Sommières watershed where the peak of the hydrograph is well
534 represented (Figure 5-a). As for Le Cailar basin, discharges calculated with CNcal are
535 almost all enclosed between both discharges calculated with the *a priori* CNs,
536 suggesting the hydrological model is well calibrated on these parts of the study area.
537 Note that the shape of Le Cailar hydrograph is not well reproduced due to the complex
538 structure of the basin through highly urbanized and irrigated. Conversely, at
539 Marsillargues (Figure 5-b), the CNcal values are systematically outside the range
540 defined by both *a priori* CNs. The CN=50 tends to underestimate the discharge for the
541 MF estimates whereas the CN=40 tends to overestimate the discharge using SPC data.
542 Simulated discharges obtained with the calibrated values show the simulations could
543 seriously be improved.

544 It is clear the results depend on the type of precipitation data used. The previously
545 presented differences in rainfall estimates represent a factor explaining the results of
546 hydrological modelling simulations. The calibrated CNcal corrects the difference
547 between both radar-based QPE (MF and SPC) and illustrates QPE are far from perfect.
548 An underestimation of rainfall is offset by a larger CN, and reciprocally. Although
549 rainfall amount based on kriging seems to be well represented at the watershed scale
550 (Fig. 4), the corresponding simulations appear to be the worst (lowest Nash efficiency).
551 In these cases, the simulated hydrographs are late in comparison with the observed ones,
552 and this problem of synchronization drastically affects the Nash efficiency computation
553 (Table 3). This can be explained by the low spatio-temporal resolution of this data, but
554 also by the rainfall-runoff model structure and calibration. The river widths that conduct

555 the transfer have been fixed and may be not adequate in this case. SPC and MF
556 estimates delivered in real time seem to better simulate the discharge. Once the bias is
557 corrected (compensated by the value of CN), the radar leads to a well representation of
558 the flood dynamics.

559 Further conclusions cannot be issued about the quality of the different QPEs because of
560 the simplicity of the hydrological model. As CINECAR only represents surface runoff,
561 it does not take into account sub-surface processes for instance. This component can be
562 significant for large basin as illustrated by the shape of the observed hydrographs. Its
563 simplification may overestimate direct runoff; that will conduct to overestimate
564 discharge on small basins where this process is prominent.

565 Nevertheless, the objective of this calibration procedure was to assess the hydrological
566 model's ability to reproduce the observed discharge and to define optimised CN for
567 each QPE. These CNcal values will be applied on the sub-basins located upstream the
568 stream gauges. They represent the best performance we can expect from the model at
569 the gauged basin scale. On the other sub-basins of the studied area (downstream
570 Marsillargues and Le Cailar basins), where no stream gauge is located, CNcal has been
571 extrapolated from the values previously calibrated on the Vistre watershed. CNcal
572 calculated with the Le Cailar stream gauge have been implemented on these sub-basins
573 for two reasons: (i) proximity because almost all these sub-basins are located in the
574 Vistre watershed, (ii) geographical similarity because they are characterized by the same
575 CN value estimated by the USDA method (USDA, 1985) using land occupation and soil
576 infiltration capacities, It is finally assumed the hydrological model with its restrictions
577 can be applied on the entire study area.

578

579
580
581

582 4-3 RIWS assessment using radar-based QPE and QPF

583 The RIWS has been applied in a framework reproducing operational conditions during
584 the night of the 29 and 30 September 2007. For each time step t_i, warnings have been
585 computed using radar estimates available on real time (for both SPC and MF services)
586 from the beginning of the storm until time step t_i, but also kriged data. To prevent from
587 the floodings that can occur in the near future, rainfall forecasts associated with both

588 radar-based QPE have been used for the four following lead times: 15, 30, 45, and 60
589 minutes. To assess the pertinence of using radar-based QPE and QPF, the RIWS has
590 been employed by testing different options: i) the susceptibility analysis has been turned
591 on and off, ii) the hydrological model has been used with *a priori* values of CN=40 and
592 CN=50, and also with the calibrated values (CNcal) defined in Section 4.2.2. The results
593 have been evaluated using the different skill scores and compared with those obtained in
594 the calibration area. They are summarized in Table 4 and the most significant are
595 represented on Figures 6.

596 *4.3.1 On the use of radar-based QPE*

597 The results obtained with kriged data are very often worse than those obtained with
598 radar-based QPE (see Table 4). Almost no inundated roads (POD=14%) are detected by
599 the RIWS with CN equal to 40. The use of the calibrated CNcal can get the best
600 discharge simulations at the location of the stream gauge, but fails in reproducing the
601 exceedance warning thresholds, especially for the intersections not located on a major
602 stream (where most of the inundations occurred). Moreover, COR scores are always
603 worse than those computed with radar-based QPE. Looking at the results in details,
604 these bad scores are due to a higher number of misses and a lower number of correct
605 warnings. The number of false alarms –similar to that obtained for radar-based QPE -
606 indicates that an underestimation of the precipitation is not solely responsible for the
607 non-detection of the inundations; otherwise, the total number of false alarms should be
608 lower. At small scale, the kriging-based interpolation of rain gauge measurements is not
609 able to represent the spatio-temporal variability of rainfall, which is essential in this
610 study. Moreover, it can be seen that the evolution of the different skill scores suffers a
611 delay of at least one hour compared to those computed from the others QPE (see Figure
612 6). This is due to the under-estimation of the first rainfall peaks (see Figure 4), and the
613 uniform distribution of the hourly data on the four 15 minutes time steps because the
614 most intense rainfall occurred at the beginning of an hour (18:00).

615 Using SPC QPE, around 80% of the flooded roads are detected with the CNcal – for
616 which the simulated discharges were the best – (see Figure 6). The scores obtained for
617 CN=50 are very similar to those calculated with CNcal and decrease when CN=40 is
618 used (POD drops to 60%). As most of the floodings were located downstream the
619 gauged basins, the detection is clearly influenced by the choice made to extrapolate the

CN values. The use of the CN adjusted on Le Cailar basin (the high value of 46) leads to simulate significant discharges, high enough to exceed the warning thresholds.

In this best case, the remaining 20% missed floodings are located on the Vistre watershed. This should not be related to a possible under-estimated precipitation on the Vistre window because the RIWS applied with MF or kriged data is also not able to detect these floodings (Figure 6). As the hydrological model seems to be able to reproduce correctly observed discharge at the Vistre gauge station, it has to be assumed that the use of an average *CN,* distributed on the entire Vistre watershed, is not adapted. The model should be influenced by the heterogeneous precipitation distribution on this watershed whose downstream part was particularly affected by the most intense rainfall. A better description of the spatial distribution of CN is probably required.

Using SPC QPE, the numbers of false alarms is very high. Indeed, they represent between 90% and 100% of the warnings delivered at the beginning of the storm, then they drop to 85% during the night. Although this ratio may seem important, the number of COR is high (close to 99%). That means despite a significant number of false alarms, the RIWS is able to rate the safe roads at the watershed scale. In order to have an overview on the whole road network, the warnings issued by the RIWS during all the storm are represented on Figure 7. 149 of the 468 existing intersections are identified as inundated sections at some point in the night (but not simultaneously). Among them, 13 correspond to effective submersions which 12 are characterized by high and significant risk. All the warnings are concentrated in areas particularly risky. That means the RIWS can capture the spatial repartition of floodings when accurate QPE are used.

Finally, the results obtained with MF QPE are less satisfactory than those obtained with SPC QPE. With a maximum of 50% for POD, the RIWS detections appear not to be satisfactory. The use of CN=40 does not permit the RIWS to deliver warnings during the night. The simulated discharges are probably too low. As rainfall estimates from MF are lower than those produced by SPC, CN has to be higher to simulate discharges susceptible to exceed the different thresholds. Setting the CN equal to 50, it is not yet sufficient and the results obtained with kriged data are still better. Only the optimised CNcal –higher than 50- gives acceptable skill scores (Fig. 6). The detected inundated roads are those located around Sommières where the estimates were the most intensive. The other inundations located a little South of Sommières and detected by the RIWS using SPC data are not identified here. As seen in Figure 2, SPC estimates tend to

653 extend the intense rainfall core to the North part of the region – as it can be confirmed
654 by kriged data, and this is not reproduced by MF data.

655 Using the three best cases (calibrated CN for MF, SPC and kriging data), the warning
656 thresholds have been reduced in order to detect all the floodings (POD=100%). It has to
657 be noticed that a reduction of 90% of the threshold was necessary to detect every
658 flooded roads, because one of the floodings was located in an area little affected by the
659 intense precipitation (see Section 4.3.3). The evolution of POD and FAR skill scores are
660 represented on Figure 8. One more time, it seems that detections using radar-based QPE
661 are more efficient that those using kriging data. For a same value of POD, FAR score is
662 always slightly lower for both MF and SPC data. Moreover, only kriging-based QPE
663 has issued 100% of false alarms, while the other QPE always issue effective warnings.
664 It could confirm that radar-based QPE better represent the spatio-temporal structure of
665 precipitation.

666 *4.3.2 On the improvement brought by QPF*

667 The use of QPF seems to be interesting in road submersion forecasting. All the results
668 offer a significant anticipation (between 15 to 45 minutes), at least during the crucial
669 steps of the event when POD highly increases, between 22:00 and 00:00. This
670 anticipation is extended to the previous time steps depending on the accuracy of the
671 QPE-based detection. Indeed, the contribution of forecasts looks being correlated with
672 the quality of the detection noticed using QPE. A better anticipation resulting from the
673 RIWS occurs when using SPC QPF, and among them, those obtained with the
674 calibrated CN (see Figure 6). When small values of CN (40) are used, SPC QPF data
675 provide less significant information. MF QPF appears to be useful only between 22:30
676 and 23:30, when they allow preventing from inundations with a lead-time of 30
677 minutes. During this short period, COR and FAR are better. Despite the propagation of
678 the convective system to the east, the use of MF QPF appears to improve the skill
679 scores, especially when the most intense precipitation occurred.

680 Regarding the best case (calibrated CN for SPC data), radar-based QPF can help to
681 detect in advance the floodings during the entire storm. Skill scores obtained with
682 QPF15 are very similar to those obtained with QPE but with an anticipation of 15
683 minutes, meaning the quality of the rainfall forecast is quite good. The use of QPF30,
684 QPF45 and QPF60 allow to detect the submersions with an advance comprised between

15 and 45 minutes, reflecting the quality of forecasts deteriorates with lead time. Regarding the response time of the concerned small watersheds (around 30 minutes), this anticipation of 45 minutes appears to be very important. In this case, the anticipation offered by simulations based on QPE is too limited to prevent from the submersion. Note the inundations detected during this anticipation time follow strictly the order of the inundations detected with the only QPE and that really occurred: starting from the submersions located on the west part on the study area until the inundations that occurred downstream the Vidourle watershed.

4.3.3 On the RIWS transfer and the use of the susceptibility analysis

Overall, the results provided for this particular storm are quite similar to those obtained for the three storms studied during the calibration step (see Versini et al., 2010a) that are summarized in Table 4 and Figure 9. On the calibration area, the good results obtained in terms of flooding detection were due to the use of the susceptibility analysis. It allowed to focus in priority the RIWS on the most vulnerable road sections without having detailed rainfall estimate. The POD score was generally higher than 85% with a COR score very close to 100%. Nevertheless, the number of false alarms was yet significant with more than 60% of the warnings issued. Without the susceptibility analysis, the accuracy of the RIWS dropped significantly with POD around to 70% and higher FAR score, reaching 100% during the event. When comparing the results obtained on calibration and current areas in ROC space, it appears that the use of susceptibility analysis in calibration area allowed to improve the number of detections while decreasing the number of false alarms. It is not the case on the Vistre/Vidourle area, where the use of the susceptibility analysis seems to not be so significant and only leads to decrease the total number of issued warnings (both correct warning and false alarms scores are lower). Although they are not represented here, the skill scores have almost the same distribution if the susceptibility analysis is used or not to characterize the road intersections (see Table 4). The good scores provided by the best case (calibrated CN for SPC data) may result from the use of spatially distributed QPE. Here, the RIWS is focus in priority on the locations where the precipitation was the most intense. Two points can be noted to explain the limit of the susceptibility analysis transfer.

When the susceptibility analysis is used, intersections characterized by a high susceptibility can be hit by a warning without the two years return period being exceeded. Most of the intersections characterized by the highest level of susceptibility are located downstream of the Vistre and Vidourle watersheds, where subcatchments are, in general, bigger and flatter. Fortunately, this part of the territory was affected by intense rainfall, and many warnings were also reported, reaching 100% of false alarms at the beginning of the event. If the storm had been further north, the results would have probably been different. Second, the flooded road classified in the safe category is not identified as potentially inundated section when the susceptibility analysis is used. It is located downstream a very small catchment of 0.95 km^2 in the upper North part of the Vidourle watershed. Here, rainfall was heavy but not sufficient to exceed the fifty years return period discharge threshold required to deliver a warning. Indeed, the simulated discharge is characterized by a two years return period. We can hypothesize that local structural problem (under-dimensioning, jam, falling tree…) could have been responsible for the flooding.

5- Conclusion

The Road Inundation Warning System developed for flash flood prone areas, and recently calibrated on the North part of the Gard region, has been applied on the South part of the Gard. Working in a framework simulating operational conditions, the RIWS has been tested to predict the inundated roads during the 29-30 September 2007 event. These results obtained for this specific storm event are very similar to those obtained in the calibration area (Versini et al., 2010b). They are promising and encourage the use of radar based spatial rainfall data. This convective storm with important spatial variability is particularly interesting to legitimate the use of the weather radar. The prototype is able to rate the inundation risk with an acceptable level of accuracy: despite many false alerts, it has a relatively high probability of detection (proportion of actually flooded points affected by a significant risk level around 80% in the best case), and a good detection of non-flooded roads (correct negative higher than 98%). From these results, some conclusions can be made on the transfer of the RIWS on a region it has not been calibrated, and on the use of radar-based QPE and QPF delivered by both services in charge of hydro-meteorological risk management.

751 The use of weather radar QPE, *a priori* more representative of the spatio-temporal
752 variability of rainfall than kriged rainfall fields based on rain gauge measurements,
753 seem to provide better results when they are not too biased. By using a simple rainfall-
754 runoff model, simulated discharges at the stream gauges have been improved by taking
755 into account the spatio-temporal distribution of rainfall as depicted from radar data.
756 Conversely, simulations using rough spatio-temporal resolution of kriged data are less
757 satisfactory. This tends to confirm the spatial variability represents a major source of
758 temporal variability in hydrological simulation (Obled et al., 1994; Sempere-Torres et
759 al., 1999). Second, the use of radar-based QPE has improved the detection of road
760 inundations. Skill scores are almost always better than those obtained with kriged data.
761 As expected, radar-based QPE allow to better represent the structure of rainfall on small
762 watersheds. When only kriged data are used, most of the non-detected inundations are
763 located downstream small watersheds with an area smaller than 10 km^2. It has been
764 noted that both services (SPC and MF) do not provide radar-based QPE with the same
765 accuracy for this particular case of the 29-30 September 2007 storm. While SPC QPE
766 show a trend to overestimate rainfall on the Vidourle watershed, both services seem to
767 describe correctly rainfall on the Vistre watershed. This conclusion is specific of this
768 particular case study and should be different for another storm.

769 Adding radar-based QPF in real time can also improve the detection of inundations,
770 especially for the cases where radar-based QPE already produced good results. In the
771 best cases, the use of QPF can anticipate the inundations with up to 45 minutes ahead.
772 This can represent valuable information from a practical point of view. Knowing that a
773 severe storm will occur (a warning has been issued few hours before the beginning of
774 intense rainfall) the road management and rescue services are prepared to intervene. If
775 they receive the information where the roads could be flooded 30 or 45 minutes before
776 it happen, they will have the opportunity to communicate and optimize the deployment
777 of its teams. For now, the RIWS prototype should therefore not be considered as a
778 decision support system but rather as a useful source of information - possibly
779 completed by field observations - that can help the emergency services during a flood
780 event to improve their decision.

781 The RIWS has shown a significant sensibility to precipitation input and rainfall-runoff
782 model calibration. Using accurate radar-based QPE, the RIWS could be used to assess
783 the results of the selected hydrological model and/or the definition of discharge

784 thresholds on ungauged basins. The results have demonstrated that the detection of
785 flooding is very sensitive to the CN values (skill scores are usually better when CN is
786 higher). The value of CN implemented on the ungauged area can also be discussed.
787 Moreover, despite the difference between both SPC and MF estimates, almost all the
788 inundated roads located on small streams of the Vistre watershed are missed, because
789 the simulated discharges did not exceed any warning thresholds. One explanation could
790 be that the average CN calibrated to simulate discharge on the main stream of the Vistre
791 basin is not sufficient to reproduce correctly the discharges (underestimated) on small
792 internal watersheds. The method proposed by Versini et al., 2010a) and calibrated on
793 the North rural part of the Gard region to estimate *a priori* a range of two CN values
794 may be unadapted here. CN values could probably be modified to take into account
795 better the specificity of the land cover (very urbanized with the presence of the city of
796 Nîmes) and the initial soil moisture. Another alternative is that theoretical return period
797 thresholds, adjusted from a large-scale study, are here overestimated. Despite the
798 intense rainfall and an acceptable simulation at Le Cailar, too few two years return
799 period threshold are exceeded. As illustrated in the study, one way to estimate new
800 discharge thresholds could be to adjust them in order to enable the RIWS to issue
801 warnings for the submerged roads that occurred in this watershed. In general, the
802 adjustment of new CN and threshold values will need additional events causing
803 floodings in this area. Particular attention should be made on the real cause of the
804 submersions in order to not to force the detection of a flooded road due to local
805 structural problem.

806 Finally, the susceptibility analysis that has been previously developed on the North part
807 of the Gard region has appeared to not be very satisfactory, for this particular event, on
808 the South part, flatter and more urbanized. Despite inundated roads are classified in the
809 highest susceptibility categories, numerous false alarms have been issued at the
810 beginning of the event by the RIWS. This is due to the location of intense precipitation
811 where intersections characterized by the highest level of susceptibility are concentrated.
812 In the downstream part, too many intersections are comprised in this category, meaning
813 discharges characterized by return periods shorter or equal to two years are sufficient to
814 flood roads. Of course it is not true, but as a consequence too many road sections are
815 identified as flooded. On the other hand, the presence of a submerged road in the safe
816 category illustrates the method could not be adapted to this part of the Gard region.

Additional future events and submerged roads should be also necessary to grow the size of the different susceptibility categories and be more conclusive. This method could be modified in function of the specific configuration of the environment, but also be completed by post-field investigations (Gaume and Borga, 2008). The characterization of susceptibly, as discharge thresholds definition, could be improved with time and accumulation of damage data.

Nowadays, the RIWS seems to have potentials for capturing timing, magnitude, and spatial repartition of the flooding risk. Using accurate QPE and QPF, it gives indications about the areas where the roads are flooded, but inside theses areas, a lot of false alarms are issued. That is why the susceptibility analysis represents a key part of the RIWS and should be improved. A good susceptibility analysis will allow to focus on the most vulnerable road sections and capture effectively the magnitude of the risk. Since no information is available on the time of inundation, we cannot conclude on the ability to capture the timing for now. The complementarity between the timing, the spatial repartition and the magnitude of the warning will make the RIWS reliable to define safe itineraries and/or prepare interventions from an operational point of view.

Acknowledgment

The study described in this paper has been carried out with the help of Meteo France and the Direction Départementale de l'Equipement du Gard which provided radar QPE and QPF data. Special thanks are due to the INPG of Grenoble and the OHM-CV (Cevennes-Vivarais Hydro-Meteorological Observatory) and especially Guy Delrieu, Laurent Bonnifait and Brice Boudevillain for providing historical meteorological data on the Gard region. The author thanks especially Eric Gaume from the Laboratoire Central des Ponts et Chaussées for sharing Prediflood project data (http://heberge.lcpc.fr/prediflood/).

Reference

Antoine, J.-M., Desailly, B. and Gazelle, F., 2001. Les crues meurtrières, du Rousillon aux Cévennes. Annales de Géographie, 110(622): 597-623.

Ayral, P.-A., 2005. Contribution à la spatialisation du modèle opérationnel de prévision des crues éclair ALTHAÏR, Université de Provence Aix-Marseille I, 310 pp.

Berenguer, M., Corral, C., Sánchez-Diezma, R. and Sempere-Torres, D., 2005. Hydrological Validation of a Radar-Based Nowcasting Technique. Journal of Hydrometeorology, 6(4): 532-549.

Borga, M., 2008. Realtime guidance for flash flood risk management.

Borga, M., Degli Esposti, S., Norbiato, D., , 2006. Influence of errors in radar rainfall estimates on hydrological modelling prediction uncertainty. Water resources Research, 42(8).

Boudevillain, B., Andrieu, H. and Chaumerliac, N., 2006. Evaluation of RadVil, a Radar-Based Very Short-Term Rainfall Forecasting Model. Journal of Hydrometeorology, 7(1): 178-189.

Bourque, L., Siegel, J., Kano, M. and Wood, M., 2007. Morbidity and mortality associated with disasters. In: Springer (Editor), Handbook of disasters research, pp. 97-112.

Bressand, F., 2002. Le projet ALHTAÏR du service d'annonce des crues du Gard. La Houille Blanche, 2: 64-68.

Cemagref, 1980. Synthèse nationale sur les crues des petits bassins versants: Méthode SOCOSE et CRUPEDIX.

Chancibault, K., Anquetin, S., Ducrocq, V. and Saulnier, G.-M., 2007. Hydrological evaluation of high-resolution precipitation forecasts of the Gard flash-flood event (8-9 September 2002). Quarterly Journal of the Royal Meteorological Society, 132: 1091-1117.

CNRS/INPG, 1997. Atlas expérimental des risques de pluies intenses, région Cévennes-Vivarais, Grenoble, France.

Cole, S.J. and Moore, R.J., 2008. Hydrological modelling using raingauge and radar-based estimators of areal rainfall. Journal of Hydrology, 358(3): 159-181.

Collier, C.G., 2007. Flash flood forecasting: GAT are the limits of predictability. Quarterly Journal of the Royal Meteorological Society, 133: 3-23.

Corral, C., Sempere-Torres, D., Revilla, M. and Berenguer, M., 2000. A semi-distributed hydrological model using rainfall estimates by radar. Application to Mediterranean basins. Physics and Chemistry of the Earth, Part B: Hydrology, Oceans and Atmosphere, 25(10-12): 1133-1136.

Creutin, J.-D. and Borga, M., 2003. Radar hydrology modifies the monitoring of flash flood hazard. Hydrological processes, 17(7): 1453-1456.

Creutin, J.-D., Borga, M., Lutoff, C., Scolobig, A., Ruin, I., Créton-Cazanave, L., , 2009. Catchment dynamics and social response during flash floods: the potential of radar rainfall monitoring for warning procedures. Meteorological Applications, 16: 115-125.

Delrieu, G., 2004. L'Observatoire Hydro-météorologique Méditerranéen Cévennes-Vivarais (The Cévennes-Vivarais Mediterranean Hydro-meteorological Observatory). La Houille Blanche, 6: 83-88.

Delrieu, G., Ducrocq, V., Gaume, E., Nicol, J., Payrastre, O., Yates, E., Andrieu, H., Ayral, P.-A., Bouvier, C., Creutin, J.-D., Livet, M., Anquetin, S., Lang, M., Neppel, L., Obled, C., Parent-du-Chatelet, J., Saulnier, G.-M., Walpersdorf, A. and Wobrock, W., 2005. The catastrophic flash-flood event of 8-9 September

2002 in the Gard region, France: a first case study for the Cévennes-Vivarais Mediterranean Hydro-meteorological Observatory. Journal of Hydrometeorology, 6: 34-52.

Dolciné, L., Andrieu, H., Sempere-Torres, D. and Creutin, D., 2001. Flash Flood Forecasting using a Coupled Precipitation Model in Mountainous Mediterranean Basin. Journal of Hydrologic Engineering 6(1): 1-10.

Gaume, E., Bain, V., Bernardara, P., Newinger, O., Barbuc, M., Bateman, A., Blaskovicova, L., Bloschl, G., Borga, M., Dumitrescu, A., Daliakopoulos, I., Garcia, J., Irimescu, A., Kohnova, S., Koutroulis, A., Marchi, L., Matreata, S., Medina, V., Preciso, E., Sempere-Torres, D., Stancalie, G., Szolgay, J., Tsanis, I., Velasco, D. and Viglione, A., 2009. A compilation of data on European flash floods. Journal of Hydrology, 367(1-2): 70-78.

Gaume, E. and Borga, M., 2008. Post-flood field investigations in upland catchments after major flash floods: proposal of a methodology and illustrations. Journal of Flood Risk Management, 1(4): 175-189.

Gaume, E., Livet, M., Desbordes, M. and Villeneuve, J.-P., 2004. Hydrologic analysis of the Aude, France, flash flood 12 and 13 November 1999. Journal of Hydrology, 286: 135-154.

Journel, A.G. and Huijbregts, C., 1978. Mining Goestatistics, Academic Press, London.

Juvanon du Vachat, R., Chèze, J.-L. and Sénési, S., 1995a. Nowcasting storms and precipitation over Ile-de-France: the Aspic project. In: A.M. Soc. (Editor), 11-th Conf. on Interactive Information Processing System for Meteorlogy, Oceanography and Hydrology, Dallas, Texas.

Juvanon du Vachat, R., Thomas, P., Bocrie, E., Monceau, G., Cosentino, P., Sénési, S., Tzanos, D. and Boichard, J.-L., 1995b. The precipitation nowcast scheme in the Aspic project, Second European Conf. on Applications of Meteorology, Toulouse, France, pp. 29-32.

Le Lay, M. and Saulnier, G.-M., 2007. Exploring the signature of climate and landscape spatial variabilities in flash flood events: Case of the 8-9 September 2002 Cévennes-Vivarais catastrophic event. Geophysical Research Letters, 34(13): 13401.

Lebel, T., Bastin, G., Obled, C. and Creutin, J.D., 1987. On the accuracy of areal rainfall estimation: a case study. Water Resources Research, 23(11): 2123-2134.

Lignon, S., 2004. Mise en place du plan d'intervention aux crises hydrologiaues (PICH) à la DDE du Gard, Ecole des Mines d'Alès, Université de Montpelier.

Moulin, L., E., G. and C., O., 2009. Uncertainties on mean areal precipitation: assessment and impact on streamflow simulations. Hydrology and Earth System Sciences, 13: 99-114.

Nash, J.E., 1969. A course of lecture on parametric or analytical hydrology. In: L. nº12 (Editor), University of Toronto.

Obled, C., Wendling, J. and Beven, K., 1994. The sensitivity of hydrological models to spatial rainfall patterns: an evaluation using observed data. Journal of Hydrology, 159(1-4): 305-333.

Ruin, I., Creutin, J.-D., Anquetin, A. and Lutoff, C., 2008. Human exposure to flash floods – Relation between parameters and human vulnerability during a storm of September 2002 in Southern France. Journal of Hydrology, 1361(1-2): 199-213.

Sempere-Torres, D., Corral, C., Raso, J. and Malgrat, P., 1999. Use of weather radar for combined sewer overflows monitoring and control. Journal of Environmental Engineering, ASCE, 125: 372-380.

946 Staes, C., Orengo, J.C., Malilay, J., Rullan, J. and No ji, E., 1994. Deaths due to flash
947 floods in Puerto Rico, january 1992 : Implication for prevention. International
948 Journal of Epidemiology, 23(5): 968-975.
949 Tabary, P., 2007. The new French radar rainfall product. Part I: methodology. Weather
950 Forecasting, 22(3): 393-408.
951 Tabary, P., Desplats, J., Do Khac, K., Eideliman, F., Gueguen, C. and Heinrich, J.-C.,
952 2007. The new French radar rainfall product. Part II : Validation. Weather
953 Forecasting, 22(3): 409-427.
954 Van Horne, M.P., Vivoni, E.R., Entekhabi, D., Hoffman, R.H. and Grassotti, C., 2006.
955 Evaluating the effects of image filtering in short-term radar rainfall forecasting
956 for hydrological applications. Meteorological Applications, 13(3): 289-303.
957 Versini, P.-A., Gaume, E. and Andrieu, H., 2010a. Application of a distributed
958 hydrological model to the design of a road inundation warning system for flash
959 flood prone areas. Natural Hazards and Earth System Sciences, 10: 805-817.
960 Versini, P.-A., Gaume, E. and Andrieu, H., 2010b. Assessment of the susceptibility of
961 roads to flooding based on geographical information – test in a flash flood prone
962 area (the Gard region, France). Natural Hazards and Earth System Sciences, 10:
963 793-803.
964 Vivoni, E.R., Entekhabi, D., Bras, R.L., Ivanov, V.Y., Van Horne, M.P., Grassotti, C.
965 and Hoffman, R.N., 2006. Extending the predictability of hydrometeorological
966 flood events using radar rainfall nowcasting. Journal of Hydrometeorology, 7(4):
967 660-677.
968 Younis, J., Anquetin, S. and Thielen, J., 2008. The benefit of high-resolution
969 operational weather forecasts for flash-flood warning. Hydrology and Earth
970 System Sciences, 5: 345-377.
971
972
973
974

975 **Figure captions**

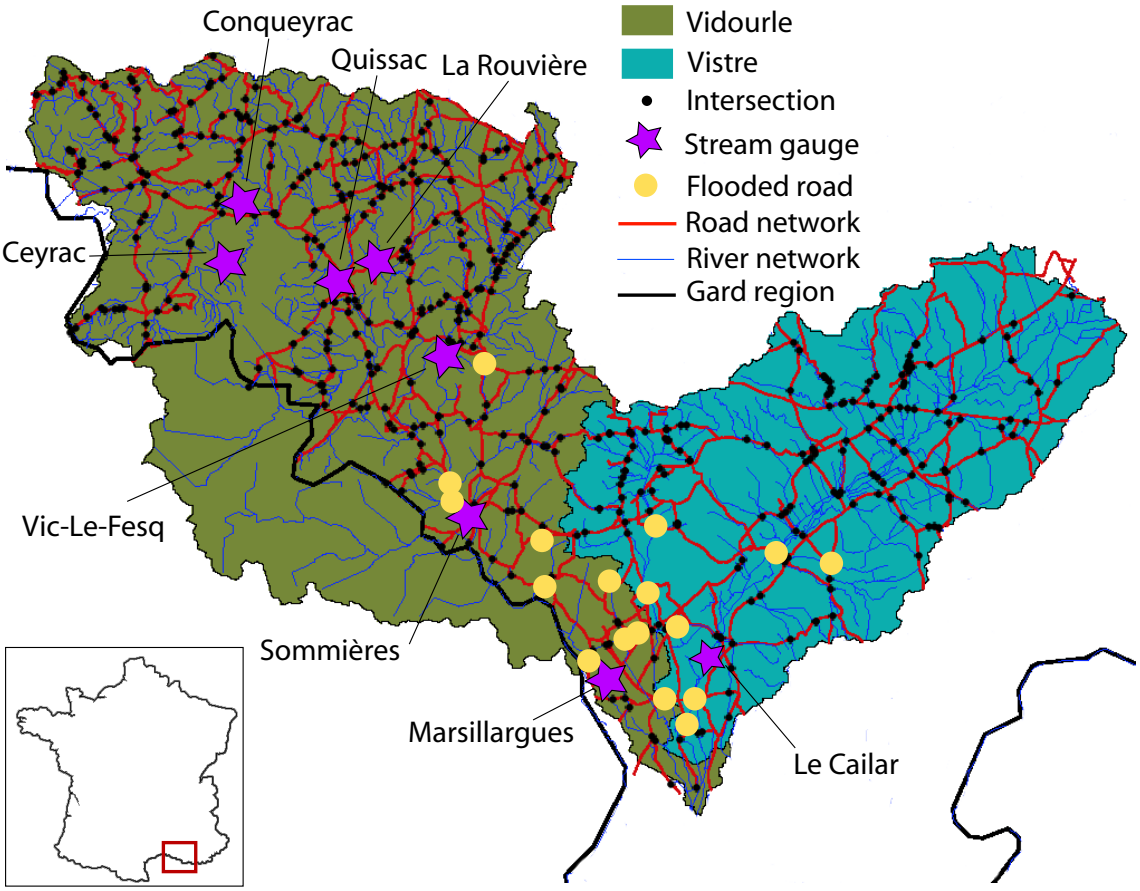

976
977 Figure 1. The Vidourle and Vistre watersheds
978

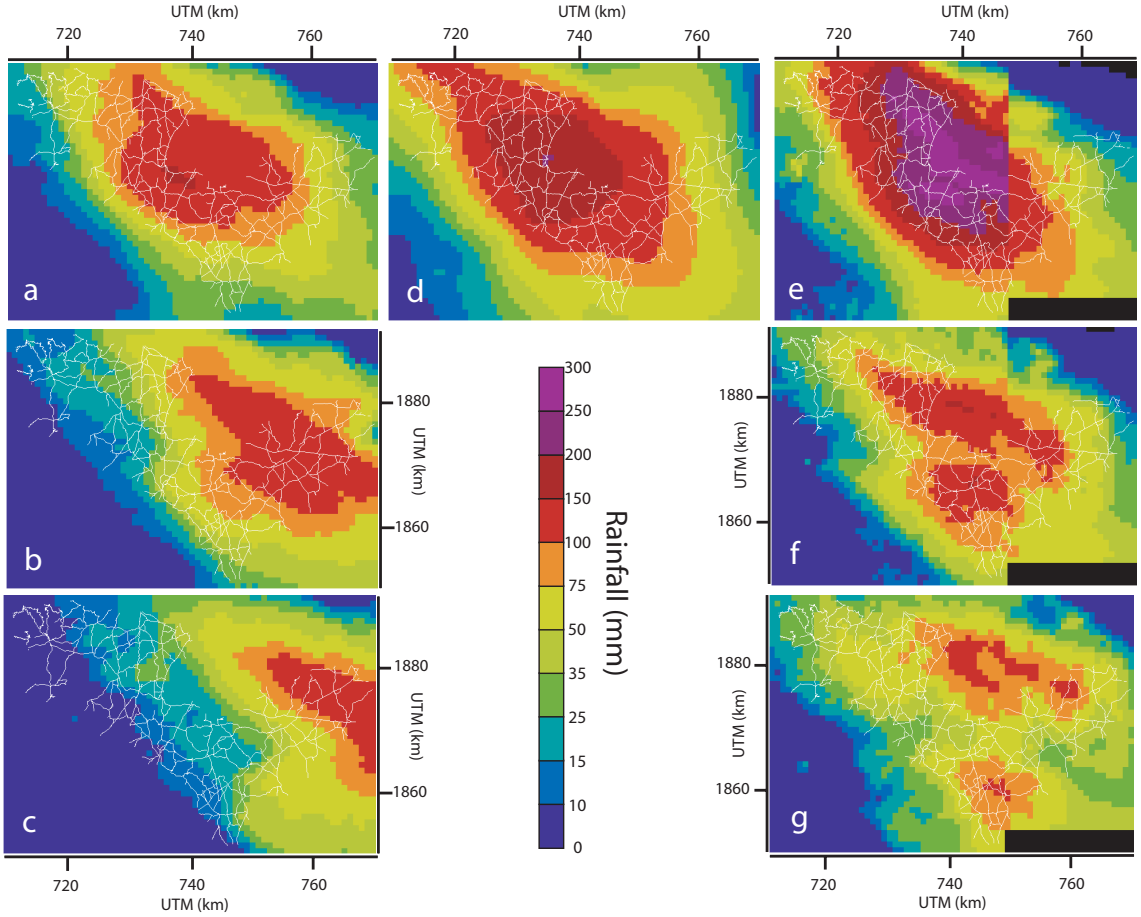

Figure 2. Rainfall accumulation: (a) MF QPE, (b) MF QPF30, (c) MF QPF60, (d) Kriging, (e) SPC QPE, (f) SPC QPF30, (g) SPC QPF60

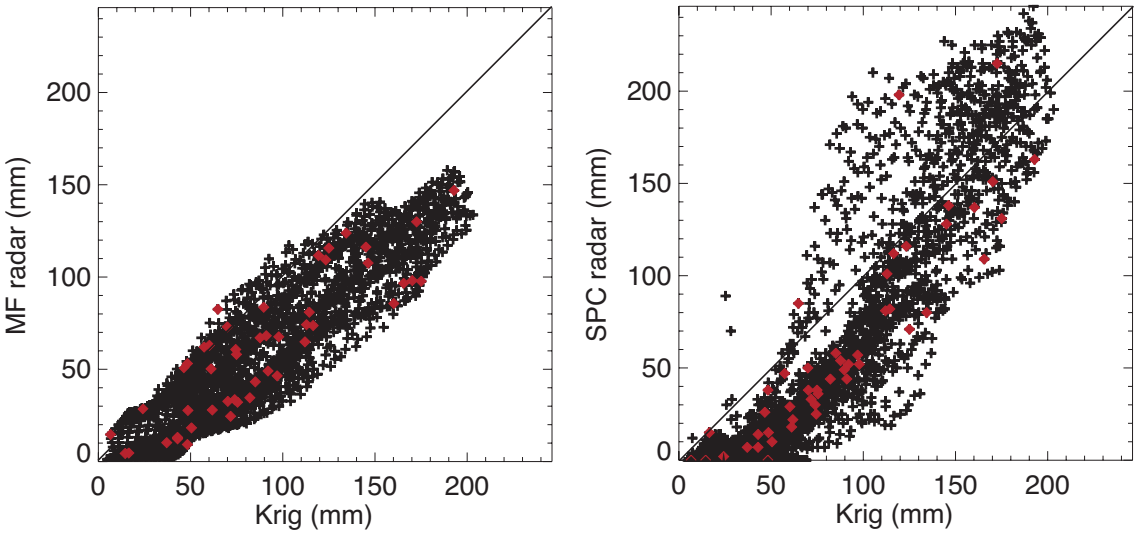

Figure 3. Scatter plots of precipitation accumulation at 1 km^2, (a) comparison between kriged data and SPC QPE, (b) comparison between kriged data and MF QPE. The red diamonds correspond to the rain gauge cells where the measure was made.

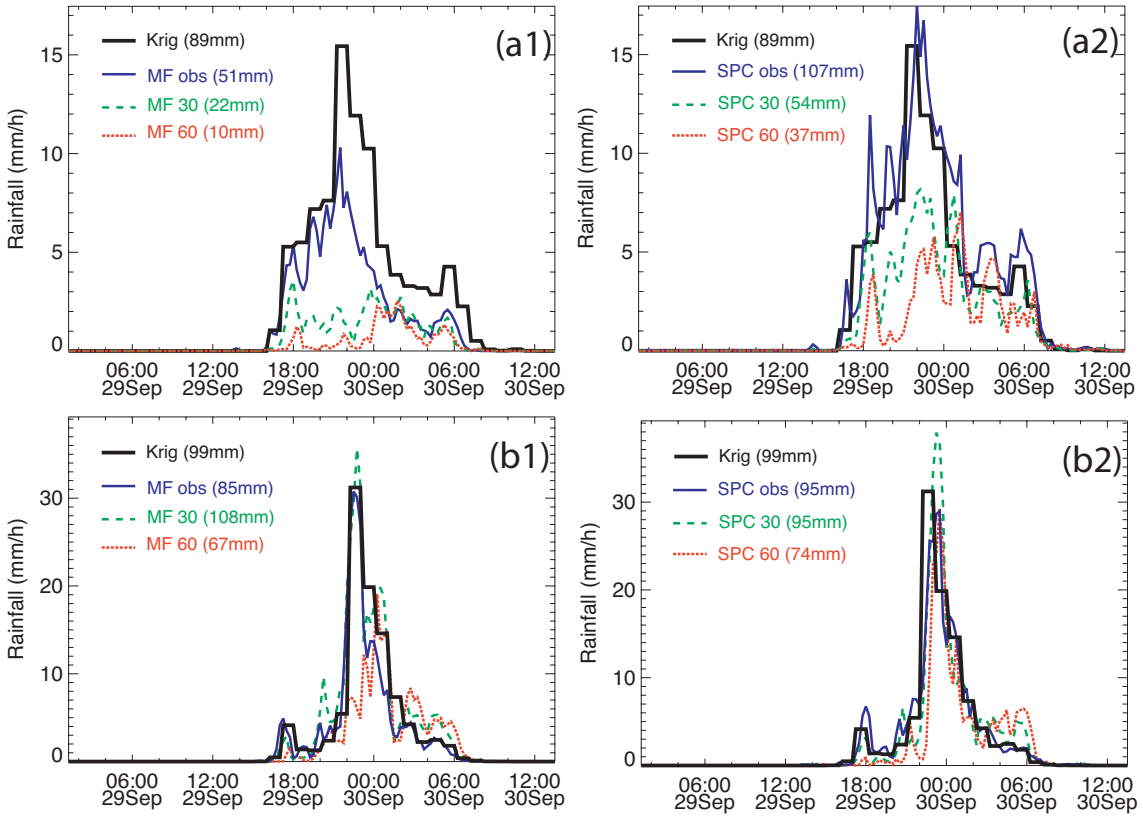

Figure 4. Rainfall hyetogram and total amount of precipitation on the Vidourle watershed (a) and on the Vistre watershed (b), for MF data (1) and SPC data (2). Precipitation estimate is represented by full line, 30 minutes forecast data by spaced dotted line, 60 minutes forecast data by small dotted line, and reference kriging data by large full line.

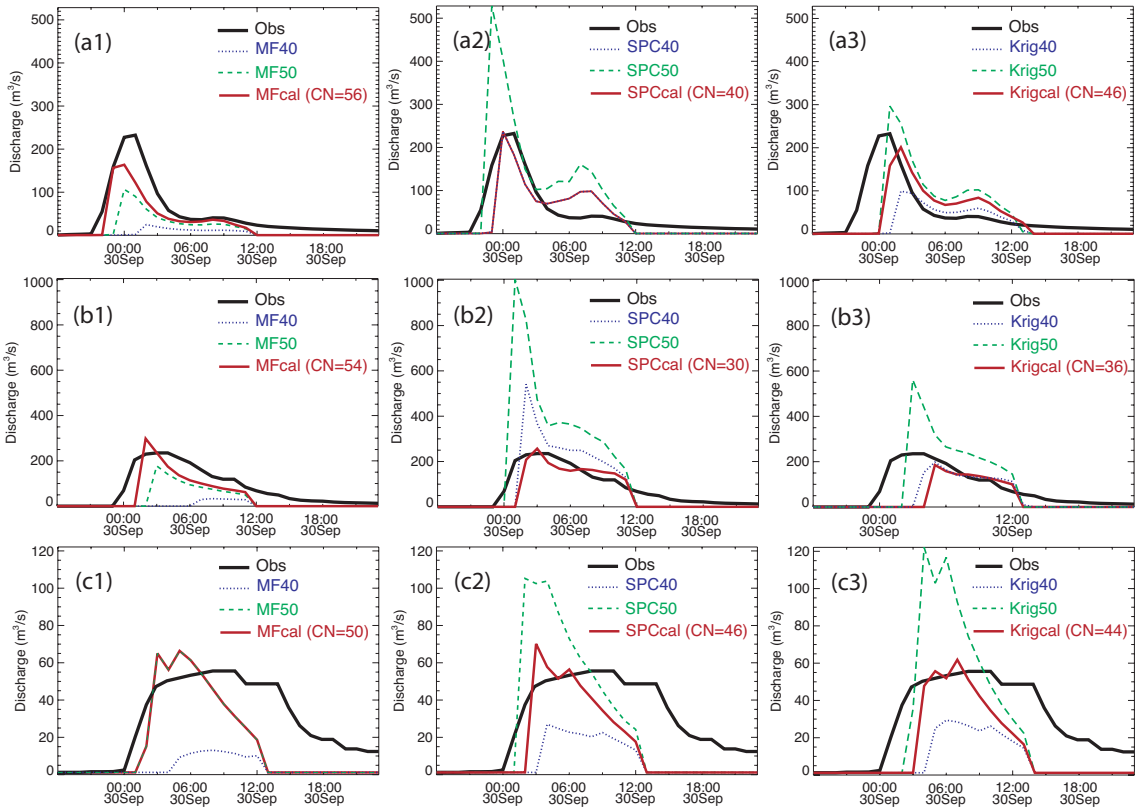

Figure 5. Discharge simulations on Sommières watershed (a), on Marsillargues watershed (b), and on Le Cailar watershed (c), using MF data (1), SPC data (2), and kriging data (3). Observations are represented by full large black line, simulations based on *a priori* CN (40 and 50) by small and spaced dotted line, and calibrated CN (the value of CNcal is written in parentheses) by full red line.

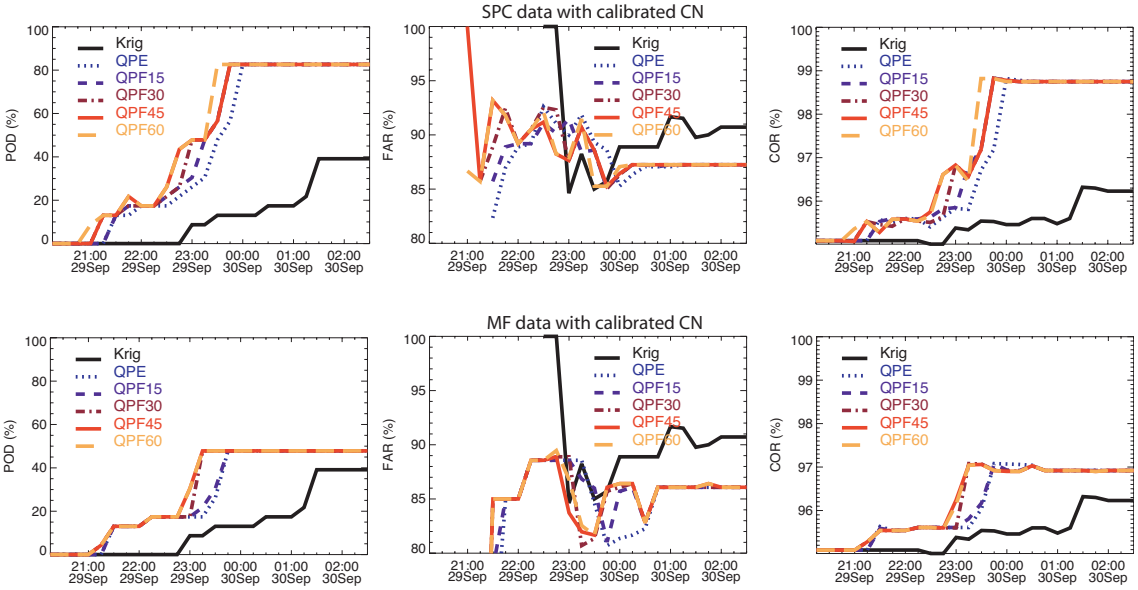

Figure 6. Skill scores for SPC data (top) and MF data (bottom) with calibrated CN. *QPE* represents the skill score calculated with the only estimations, *QPF15* those with the 15 minutes forecast added, respectively *QPF30*, *QPF45*, *QPF60* with the 30, 45, and 60 minutes forecasts added. Finally, *Krig* represents the skill score computed using kriged data

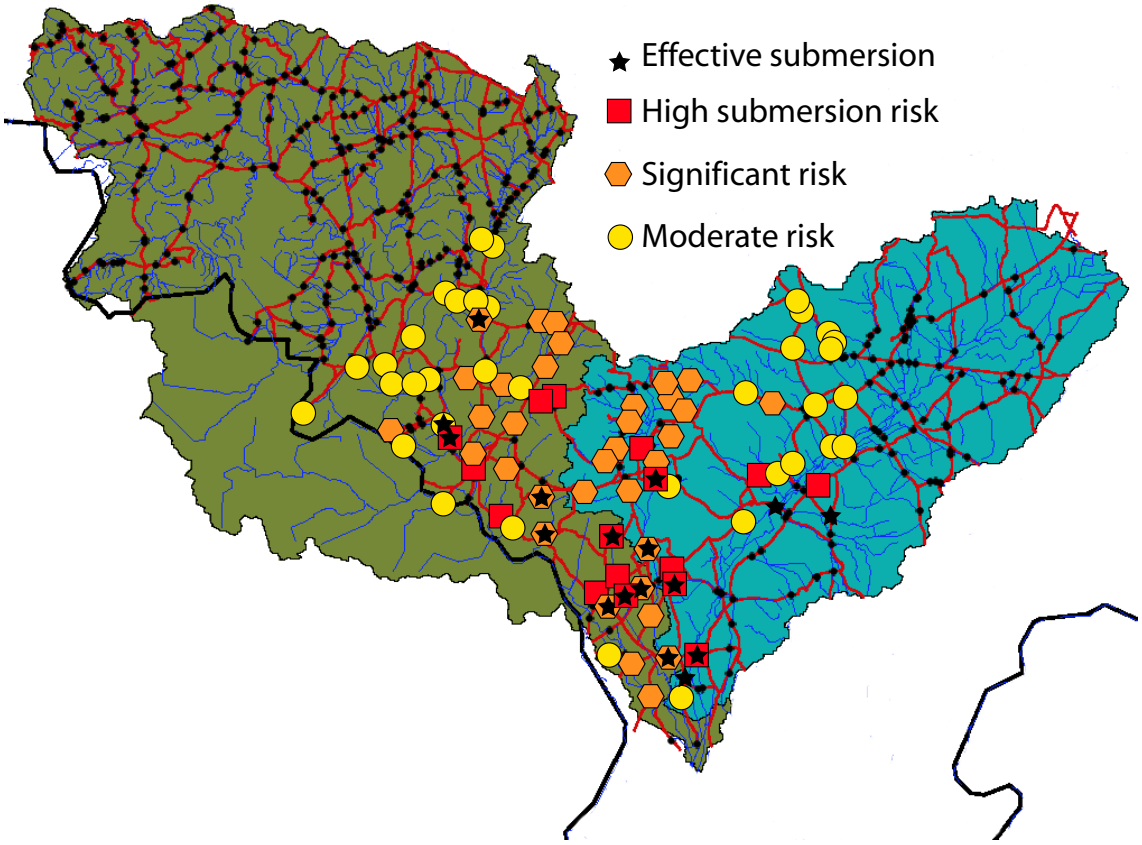

Figure 7. Warnings issued by the RIWS during all the event using SPC QPE, CNcal and the susceptibility analysis

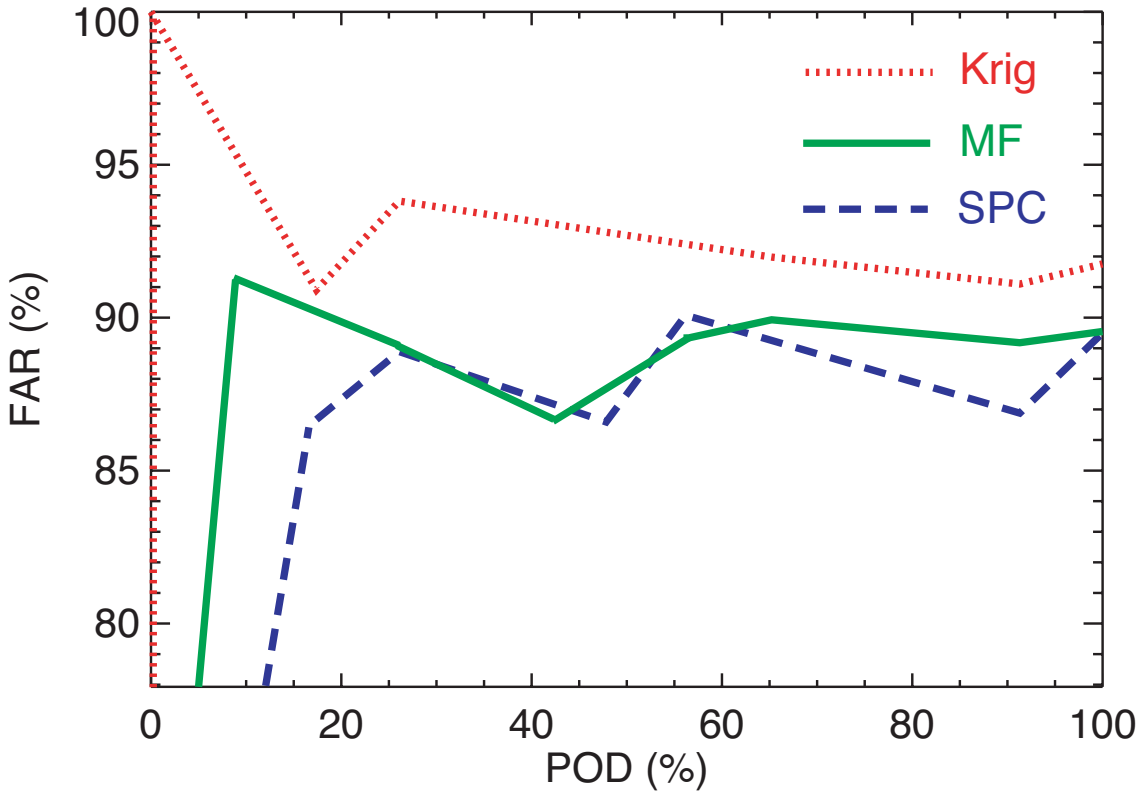

Figure 8. Evolution of FAR and POD skill scores reducing the warning threshold for kriging, MF and SPC QPE using the calibrated CN.

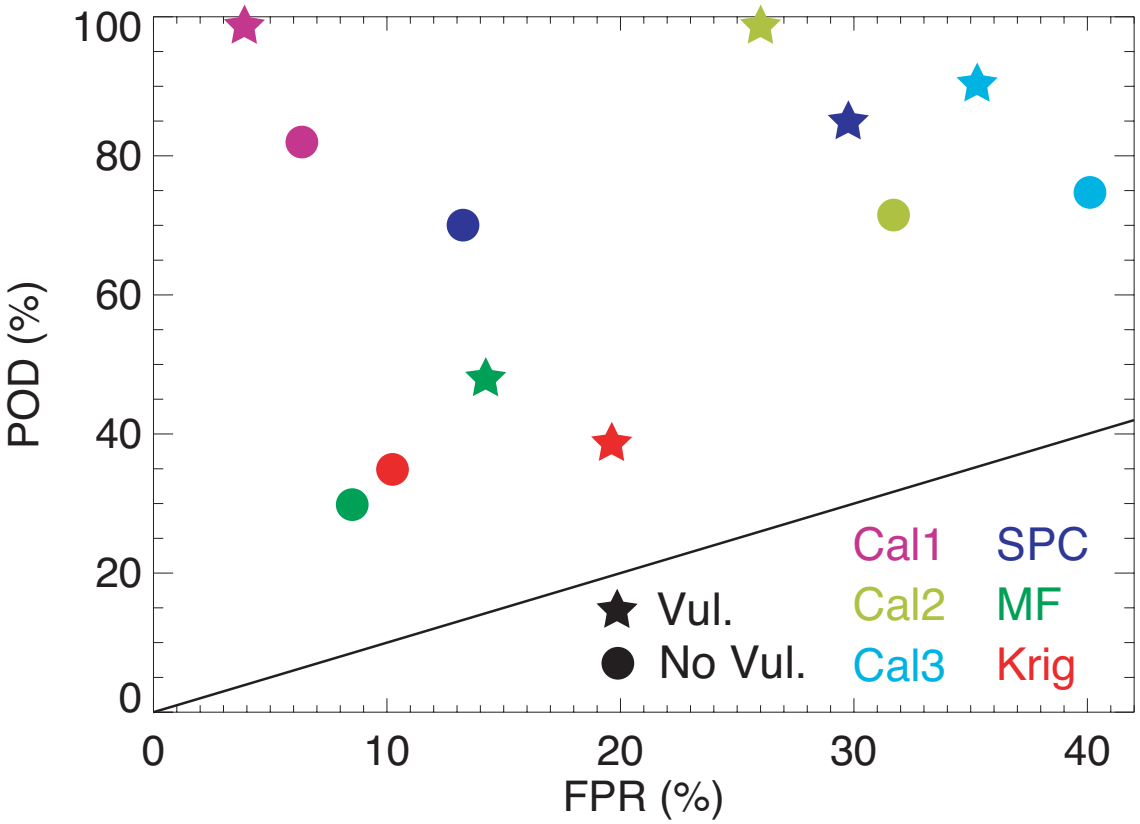

Figure 9. Inundation forecasts represented in the ROC space. The results obtained for the 3 calibration events (Cal1, Cal2 and Cal3) are compared to those computed with SPC, MF, and Krig QPEs. POD and FPR values are calculated using the total number of correct warnings and false alarms issued during the event.

Table captions

	$Q_2/2<Q_{sim}<Q_2$	$Q_2<Q_{sim}<Q_{10}$	$Q_{10}<Q_{sim}<Q_{50}$	$Q_{sim}>Q_{50}$
Susceptibility High	SR	HSR	HSR	HSR
Susceptibility Medium	MR	SR	SR	HSR
Susceptibility Low	No risk	MR	MR	SR
Safe	No risk	No risk	No risk	MR
No susceptibility analysis	No risk	MR	SR	HSR

Table 1. Risk levels based on exceeded discharge thresholds – with susceptibility category or without

Category of susceptibility	Calibration area	Study area	Submerged intersections
High	8%	12%	35%
Medium	22%	20%	30%
Low	54%	50%	30%
Safe	16%	18%	5%

Table 2. Repartition of the road sections between the four susceptibility categories using the road susceptibility rating method applied on the previous calibration area, on the Vistre and Vidourle area and on the 29-30 September 2007 storm flooded road

	SPC40	SPC50	SPCcal	MF40	MF50	MFcal	Krig40	Krig50	Krigcal
Sommières	0.81	-0.65	0.81	-0.18	0.44	0.73	0.00	-0.13	0.28
Marsillargues	0.19	-4.05	0.70	-0.32	0.40	0.67	0.18	-0.19	0.35
Le Cailar	0.03	-0.06	0.39	-0.26	0.43	0.43	0.10	-0.24	0.37

Table 3. Nash efficiency for discharge estimation using CN=40, CN=50 and CNcal for the following watersheds: Sommières (a), Marsillargues (b), and Le Cailar (c)

	SPC			MF			Krig			***Cal***
	40	50	Cal.	40	50	Cal.	40	50	Cal.	
POD	60.2/56.5	82.6/78.3	82.6/69.6	0/0	34.8/17.4	47.8/30.4	14.0/0	58.3/50.1	39.1/34.8	***76.0/96.0***
COR	97.8/97.6	98.8/98.6	98.8/98.2	95.2/95.4	96.5/95.7	97.1/96.2	95.5/0	97.3/97.1	96.3/96.3	***96.3/98.2***
FAR	90.2/75.5	87.3/84.8	87.2/78.4	0/0	86.7/90.0	86.1/85.4	86/100	87.3/89.5	93.7/87.7	***63.0/73.0***

Table 4. Summary of the RIWS maximum skill scores for the different types of QPE (SPC, MF and kriged data) and different CN values. The left value is computed without considering the susceptibility analysis, the right one considering the susceptibility. The last column contains the average results obtained in the calibration area for 5 events.